The value 36.92 Mev given by Friedlander et al.[4] is used for the Q of the free Λ^0 decay.

Within the error of charge and mass there exists alternate possible interpretation of the disintegration scheme of the hyperfragment. The following alternate reactions have been considered:

$$_\Lambda He^5 \rightarrow H^2 + H^3 + Q_2, \qquad (2)$$

$$_\Lambda He^5 \rightarrow H^3 + H^1 + n + Q_3, \qquad (3)$$

$$_\Lambda He^3 \rightarrow H^1 + H^2 + Q_4. \qquad (4)$$
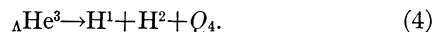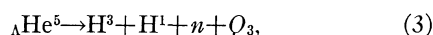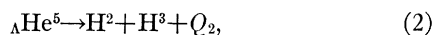
Reaction 2 was rejected because of the lack of momentum balance between H^2 and H^3. If we assume the variation in linearity between the proton and triton in the vertical plane to be due to a neutral particle, reaction 3 is possible. The emission of a neutron must

be assumed to balance momentum. The energy of the proton from grain count was found to be 124 ± 12 Mev. This would permit a neutron to have an energy range of $0.4 - 2$ Mev, where 0.4 Mev would give a Q value of 169 Mev, while 2.0-Mev neutrons would give a Q value of about 159 Mev. Reaction 4 is not admitted by theory.[3]

The results of 4.3 ± 1.6 Mev for the binding energy of Λ^0 in a nonmesonic decay of $_\Lambda He^4$ is in agreement with that found from the charged mesonic decays reported by others.[3,5,6]

The authors are very grateful to Professor Marcel Schein of the University of Chicago for his generous assistance in regard to this problem, and to Dr. W. F. Fry of the University of Wisconsin, for his very helpful and stimulating discussions.

[4] Friedlander, Keefe, Menon, and Merlin, Phil. Mag. 45, 533 (1954).

[5] Hill, Salant, Widgoff, Osborne, Pevsner, Ritson, Crussard, and Walker, Phys. Rev. 94, 797(A) (1954).

[6] Naugle, Ney, Freier, and Cheston, Phys. Rev. 96, 1383 (1954).

Masses of Identified Positive Heavy Mesons*

James Ray Peterson†
Radiation Laboratory, University of California, Berkeley, California
(Received October 8, 1956)

The charged secondary particles from all presently known decay modes of positive K mesons have been identified, and the masses of the primaries measured by the momentum-range method. More than 2000 K mesons were found in a rather large stack of nuclear emulsion after its exposure, behind the strong-focusing magnetic spectrometer at the Bevatron, to a target plunged into the 6.2-Bev circulating proton beam. The mean K-meson momentum at the stack was 360 Mev/c, and the proper time of flight was 1.4×10^{-8} sec. The masses of 263 systematically selected K mesons were measured, and the averages for the various decay modes are

$$M(\tau + \tau') = 966.6 \pm 1.9m_e, \quad M(K_{\pi 2}) = 966.9 \pm 2.0m_e, \quad M(K_{\mu 2}) = 967.2 \pm 2.2m_e,$$
$$M(K_{\mu 3}) = 969 \pm 5m_e, \quad M(K_{\beta 3}) = 967 \pm 8m_e.$$

The standard errors indicated apply to the relative masses; the uncertainties on the absolute masses are slightly larger. Various corrections are described. The results are discussed in the light of recent ideas concerning heavy-meson characteristics.

I. INTRODUCTION

THE existence of at least six different decay modes available to positive K mesons (see Table I) has given importance to mass measurements on the mesons as a means of determining whether a single particle is ultimately responsible for all modes of decay or if there is more than one distinct parent.

Two general approaches to the determination of the mass of an unstable particle have been employed in the investigation of K mesons. The Q-value method deduces the mass of the parent meson from a measurement of the total kinetic energy of the decay and a knowledge

of the rest masses of the secondaries. This method can be used if all secondaries are charged, as in the τ or in the cases of two-body decay, such as the $K_{\pi 2}$ and $K_{\mu 2}$. The second approach is to measure various

TABLE I. Modes of decay of positive K mesons.

Type	Name	Decay mode
$K_{\pi 3}^+$	τ^+	$\tau^+ \rightarrow \pi^+ + \pi^+ + \pi^-$
	τ'^+	$\tau'^+ \rightarrow \pi^+ + \pi^0 + \pi^0$
$K_{\pi 2}^+$	θ^+, χ^+	$K_{\pi 2}^+ \rightarrow \pi^+ + \pi^0$
$K_{\mu 2}^+$		$K_{\mu 2}^+ \rightarrow \mu^+ + \nu$
$K_{\mu 3}^+$	κ	$K_{\mu 3}^+ \rightarrow \mu^+ + 2$ or more neutral particles[a]
$K_{\beta 3}^+$		$K_{\beta 3}^+ \rightarrow \beta^+ + 2$ or more neutral particles[b]

[a] Yekutieli, Kaplon, and Hoang [Phys. Rev. 101, 506 (1956)], have found an electron pair emitted from an otherwise typical $K_{\mu 3}$ ending, which suggests the presence of a π^0 in some cases.
[b] The exact composition of the neutral particles here is not known.

dynamical characteristics of the K particle itself before it has decayed, and shall be referred to as a *primary-mass* measurement. It can obviously be used regardless of the decay mode. The two methods should yield the same results unless the primary K meson has undergone an undetected energy transition to a lower state (the immediate parent) which has then decayed according to the observed mode.[1] In this case the Q-value determination should yield a mass value lower than the primary mass by an amount equal to the energy released in the undetected transition.

The mass of the τ was known to be close to $965m_e$ from a Q-value determination as early as 1951.[2] However, prior to 1955, the results of measurements on the other positive K-meson masses were confusing.[3] They were generally primary mass determinations based on measurements of specific ionization and multiple scattering as functions of range in emulsion, methods that are unfortunately subject to significant systematic errors as well as low statistical weights. There were some apparent inconsistencies among these emulsion data as well as some of the early cloud chamber results[3,4] based on both Q-value measurements and momentum-range evaluations of the primary mass.

At the Pisa Conference in July, 1955,[5] results were presented that considerably clarified the situation. The large "G" stack[6] had been exposed to cosmic rays in October 1954 by a group of collaborating European laboratories and was designed to obtain Q-value measurements for the $K_{\mu2}$ and $K_{\pi2}$ by actually stopping the secondaries in the emulsion and accurately measuring ranges. Furthermore, accurate determination of the relative masses of all the various K^+ particles had been made possible at the Berkeley Bevatron in early 1955 by the development of the strong-focusing spectrometer.[7] In addition to increasing the scanning efficiency in emulsion by a factor of 100, this system allowed the application of the momentum-range method to primary mass measurements in emulsion. Both the "G" stack data[6] (range of secondaries) and the results from the Bevatron[8] (momentum-range of primaries) placed the masses of the $K_{\mu2}$ and the $K_{\pi2}$ equal to that of the τ to within $15m_e$. In addition the momentum-

range measurements gave the $K_{\mu3}-\tau$ mass difference to be $12\pm16m_e$.

On the other hand, the analysis[9] of all existing data on τ decays indicated different spin-parity configurations for the $K_{\pi2}$ and τ. The Pisa Conference thus pointed to a situation wherein there might exist a fundamental difference between the mesons parent to the $K_{\pi2}$ and the τ-decay products with no measurable mass difference attendant. It made manifest the need of further, more precise, measurements on all observable characteristics of the K^+ mesons.

The experiment described herein was designed to reduce the errors in the relative and absolute primary-mass values of identified K^+ mesons by means of the momentum-range method and is part of a general investigation of positive heavy mesons, the results of which are being published elsewhere.[10,11]

II. EXPERIMENTAL PROCEDURE

A. General Method

A momentum-range determination of the mass of a charged particle is based on well-established relationships that are known to describe the range of a particle of given charge, mass, and momentum. In general, a measure of the momentum is achieved through a knowledge of the particle's charge and its trajectory in a magnetic field through which it passes before entering the stopping medium or detector in which the range is measured.

In the case of the strong-focusing spectrometer, shown schematically in Fig. 1, the particles are somewhat collimated before entering the magnetic field. If the magnetic field is directed vertically, all particles entering any particular vertical section of the detector are characterized by a small band of momenta whose width is inversely proportional to the resolution of the system and whose average value is determined by the value of the magnetic field and the radius of curvature of the corresponding average trajectory. The momentum characteristic of a given entrance position is evaluated from a measurement of the average range of a particle of known mass (e.g., the proton) that has entered the detector at that point. The relative momentum spread obtained in this experiment was about 1% and is discussed in Appendix D.

B. Experimental Apparatus and Details of the Exposure

The essential elements of the strong-focusing magnetic spectrometer are shown in Fig. 2. A target was

[1] S. B. Treiman and H. W. Wyld, Jr., Phys. Rev. **99**, 1039 (1955); T. D. Lee and J. Orear, Phys. Rev. **100**, 932 (1955).

[2] Fowler, Menon, Powell, and Rochat, Phil. Mag. **42**, 1040 (1951).

[3] Report of the Committee on K particles, Padua Conference, Suppl. Nuovo cimento **12**, 433 (1954).

[4] Gregory, Lagarrigue, Leprince-Ringuet, Muller, and Peyrou, Nuovo cimento **11**, 292 (1954).

[5] Report on the Pisa Conference on Elementary Particles, 1955, Suppl. Nuovo cimento (to be published).

[6] "G Stack Collaboration Experiment (1954)," Nature **175**, 971 (1955); also Nuovo cimento **2**, 1063 (1955).

[7] Kerth, Stork, Birge, Haddock, and Whitehead, Phys. Rev. **99**, 641(A) (1955).

[8] Birge, Peterson, Stork, and Whitehead, Phys. Rev. **100**, 430 (1955); Birge, Haddock, Kerth, Peterson, Sandweiss, Stork, and Whitehead, Suppl. Nuovo cimento (to be published).

[9] E. Amaldi, Mimeographed Report on the Pisa Conference, 1955, p. 1.

[10] R. P. Haddock, Nuovo cimento **4**, 240 (1956). Also University of California Radiation Laboratory Report UCRL-3284, February, 1956 (unpublished).

[11] Birge, Perkins, Peterson, Stork, and Whitehead, Nuovo cimento **4**, 834 (1956).
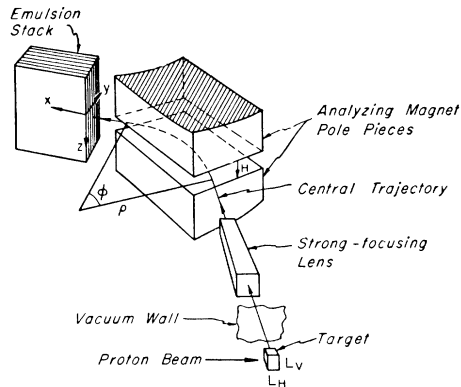
FIG. 1. Sketch of the basic experimental arrangement, indicating the coordinate system assigned to the emulsion stack.

FIG. 2. The strong-focusing spectrometer.

plunged into the 6.2-Bev proton beam in one of the straight sections of the Bevatron. Particles of proper charge and momentum coming from the target at 90° to the incident beam passed through the 0.090-inch aluminum wall of the Bevatron vacuum tank and through a compound lens formed by a series of quadrupole magnets, and were brought to a focus in a stack of nuclear emulsions placed behind a momentum-analyzing magnet. The flux of positively charged particles consisted mainly of protons, K mesons, and pions. The momentum selection of the analyzing magnet restricted the protons entering the stack to ranges typically in the vicinity of 1.5 cm and the K mesons to about 7 cm, while the pions passed completely through the stack. Brass was placed on the low-energy side of the magnet to shield the detector from neutral radiation from the target, and a considerable amount of lead and concrete was also used to shield from secondary radiation associated with beam "spill-out" during the early part of the accelerating cycle. The copper target used was $\frac{3}{8}$ in. high and $\frac{5}{8}$ in. in the proton beam direction. The aperture of the lens was 2 inches and the analyzing magnet had a 2.5-in. gap.

In order to obtain sufficient strength in the lens it was necessary to use four quadrupole magnets. The first two formed a lens converging vertically and diverging horizontally, while the last two magnets were operated so as to diverge vertically and converge horizontally. The compound lens formed by these two elements was both vertically and horizontally convergent; however, it was astigmatic. Since the momentum resolution of the system was determined principally by the horizontal size of the target image at the stack (see Appendix D), there was an incentive to minimize the horizontal magnification to a value that was satisfactory in consideration of the concomitant increase in the vertical magnification. If the latter became too large, particles would be lost by striking the pole pieces of the analyzing magnet. The horizontal magnification used was about 0.6×, and the vertical magnification was about 1.5×. It turned out that a significant number
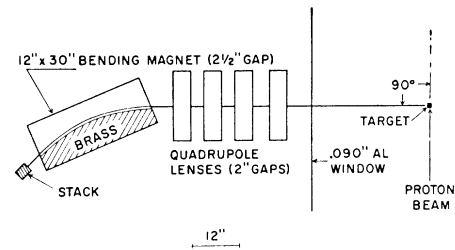
of particles did in fact strike the pole pieces. The particle density spectrum in the stack, taken in a direction perpendicular to the plane of the pole faces, showed a sharp cutoff on one end corresponding to the shadow of the top pole piece. This was apparently caused by a vertical misalignment of the lens "telescope" and perhaps by a poorer-than-expected vertical focus.

Proper current values for all the magnets were obtained from a series of wire-trajectory measurements made for particles of momenta in the vicinity of 360 Mev/c. This method was found to be quite satisfactory in achieving proper focus and magnification conditions. The measurements were made considerably easier and more accurate after the construction by Mr. Leroy Kerth of a current regulator which compensated for currents induced in the wire by motion in the magnetic field.

The trajectories obtained from these wire measurements were used to position the stack when the exposure was made, so that the particles would enter approximately perpendicular to the front face of the stack. If we assign rectangular coordinates to the detector such that the z axis is in the direction of the magnetic field and the x axis represents the average direction of the particles entering the detector, the stack is oriented with the plane of the emulsion lying in the x-z (vertical) plane as shown in Fig. 1. The y axis is in the direction of increasing particle momentum. The stack was placed so that the particles entered the middle of the long (17.5-in.) side, thus allowing enough emulsion above and below the beam to stop the muons from the $K_{\mu 2}$'s that decayed in these directions.

The emulsions were clamped firmly between two sheets of Bakelite 0.75 in. thick, and all four sides of the stack were milled flat. This allowed a fairly accurate determination of the volume of the stack and thus of its density, and in addition presented a smooth surface to the incident particles for an accurate range measurement. Fiducial marks for aligning the emulsions were provided at various points by exposing the milled sides to x-rays passed through a slit system. When developed, each emulsion thus contained a set of 18 black lines about 25 μ wide, extending about 0.5 inch into the emulsion.

After processing, the glass-mounted emulsions were cut parallel to the x axis (short dimension) into three
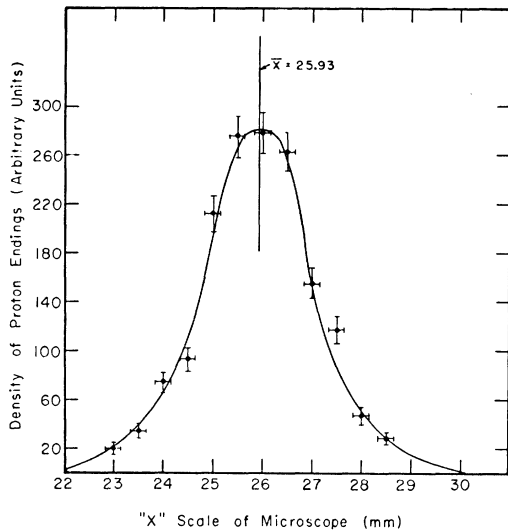
FIG. 3. A typical proton-ending distribution (plate 75).

equal sections for ease in scanning. The center plates contained the incident particles, while some of the K-meson secondaries went into the side sections.

C. Determination of the Proton Momenta

1. Measurement of the Projected Ranges

The stack was oriented so that the plane of the emulsions was parallel to the momentum-analyzing magnetic field; thus the average momentum of all particles entering a particular emulsion could be represented as a function of the index number of that emulsion, the numbers running from 1 to 95 in the direction of increasing momentum. The momentum variation across the stack was obtained from the projected ranges of the protons in eight plates. Since the absolute mass value obtained by this method is quite sensitive to the value of the estimated initial momentum, considerable effort was made to achieve an accurate representation of the proton range distribution in the stack. The average projected range was measured by determining the density of proton endings in strips 330μ wide. These strips spanned the distribution of endings in a given plate. The range distributions were characterized by a root-mean-square deviation of about 6.5%, resulting from effects discussed in Appendix D. A curve was drawn to best fit each distribution, and the median range was taken as that corresponding to the peak value of the curve. A typical example of the distribution of proton endings in a single plate is shown in Fig. 3.

It was necessary to make certain modifications to these values before the incident-proton momentum could be obtained.

2. Corrections to the Measured Projected Ranges

(a) Range shortening due to scattering.—The measured projected range was shorter than the true range along

the track because of the multiple scattering incurred while the protons were slowing down in the emulsion. The average shortening for protons of a particular range was calculated by a method described in Appendix A, and this quantity was then added to the measured projected range. The effect amounted to about 0.5% of the total range and varied slightly across the stack.

(b) Effect of the entrance angle.—It follows from the geometry of the apparatus that an "average" particle would enter perpendicular to the face of the stack at only one lateral (y) position, the remainder either climbing or diving in the emulsion when viewed on the microscope. This small but quite significant effect both shortened the projected range and created a difference between the entrance plate and the plate in which the protons actually came to rest. The correction is described in Appendix B.

(c) Effect of the air path.—The above corrections afforded an accurate description of the true average proton range $R_{0P}(y)$ and momentum $p_{0P}(y)$ as a function of the entrance position y as shown in Figs. 4 and 5, respectively. However, in order to arrive at a quantity relating to the true average K-meson momentum $p_{0K}(y)$, which was of actual interest, it was necessary to correct for the difference between p_{0K} and p_{0P} in each plate. This difference resulted from the different rates of energy loss experienced by the mesons and protons in the air path between the entrance to the analyzing magnet and the emulsion stack. As a result of the correction, a modified proton range curve was constructed to represent the ranges $R_{0P}(p_{0K})$ for protons of momentum equal to the average K-meson momentum as a function of entrance position at the
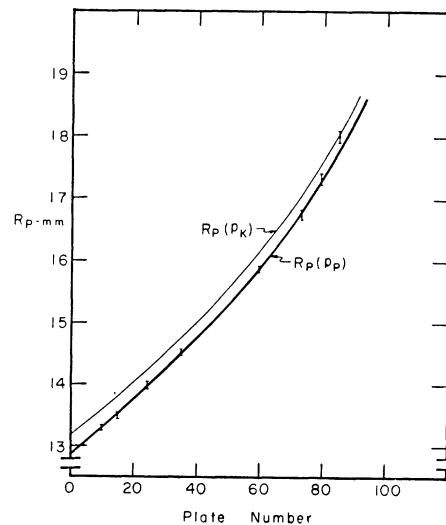
FIG. 4. The corrected proton range curves $R_P(p_P)$ and $R_P(p_K)$ vs entrance-plate number. The upper curve was used to represent the K-meson momentum p_K in the mass determination as indicated in Fig. 7. (All measured K particles entered in Plates 10 to 87.)

stack. This curve has been included in Fig. 4. The correction is described further in Appendix C.

D. Scanning for the K Mesons

K mesons entered the emulsion with a relative ionization about 1.8 times minimum. A swath perpendicular to the incident-particle direction, and about 1 cm behind the stopping protons was scanned for tracks whose grain densities were estimated to be from 1.5 to 3 times minimum and whose directions lay within about 15° of that of the x axis. Such tracks were followed to their endings. The observation of one or more secondary tracks at the end point identified the primary as a K meson. The average K-meson track was thus followed for about 4 cm. This procedure allowed a reasonably uniform efficiency for the observation of particles of mass 800 to 1150 electron masses. Pions were at minimum ionization and were not followed.

E. Identification of the Modes of Decay

Almost all tau mesons, with their striking three-prong decay, were identified at once by the scanners. Furthermore, the scanners followed to their endings all other secondaries recognized as being of low energy. In this manner most of the low-energy decay τ''s and some $K_{\mu3}$'s were identified. Systematic identification of all other events was accomplished either by following the secondaries or by a blob count taken either near or at some distance from the decay point. These methods are described in detail elsewhere.[11]

Of those particles whose masses were measured, all τ's, τ'''s, $K_{\mu3}$'s, $K_{\beta3}$'s, 32 $K_{\pi2}$'s, and 60 $K_{\mu2}$'s were positively identified by methods other than the simple blob count near the decay point. The results of the latter method are shown in Fig. 6. Shaded areas correspond to secondaries also identified by other methods. Events lying in the 4% overlap region between the $K_{\mu2}$ and
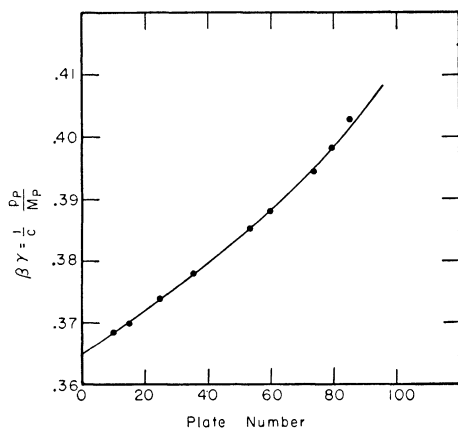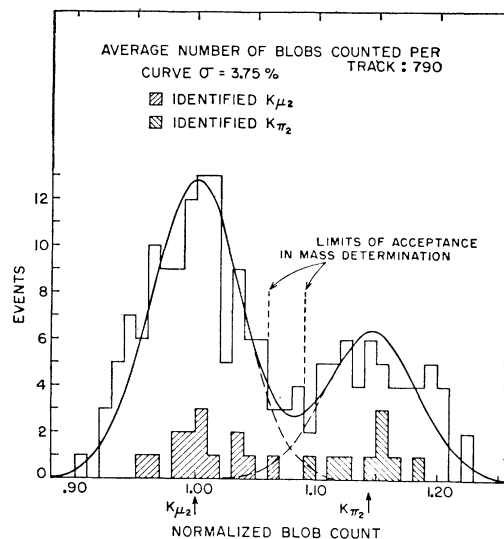
FIG. 6. Normalized results of blob counts made on K_L secondaries near the point of decay. Average number of blobs counted per track: 790. Curve = 3.75%.

$K_{\pi2}$ distributions were eliminated in the selection of events for mass measurement. The remainder were considered to be either $K_{\mu2}$'s or $K_{\pi2}$'s. It was thought that the small number of $K_{\mu3}$ and $K_{\beta3}$ modes that might contribute to the main $K_{\pi2}$ and $K_{\mu2}$ blob count distributions would not be sufficient to significantly affect the mass values obtained with their inclusion. Forty $K_{\mu2}$'s and twenty-eight $K_{\pi2}$'s from their respective blob-count groups were used in the mass measurements.

F. Measurement of the K Ranges

After the decay mode of a meson had been identified, the range of the primary meson was measured. The following procedure was selected as the most accurate method of determining the true ranges of the particles, considering the general character of their tracks. Most of the tracks were within 10° of being parallel to the x axis in the emulsion, which was one of the two directions of motion of the microscope stage. Each track was followed backward from the point of decay. Coordinates (x_i, y_i, z_i) were recorded for each point where there had accrued a change in direction (from that of the previous point) greater than about 3°. The range was then obtained essentially from the sum of the chord lengths that were computed from these sets of coordinates. This method avoided errors due to random misalignment of the emulsions (which was less than 25 μ), air gaps,[12] and "rub-off" or other similar losses of parts of the tracks near the surfaces of the emulsion. Occasional systematic error in the computed total range was negligible. Statistical errors were very small (less than 100 μ) compared to the range straggling.

FIG. 5. Incident proton momentum p_P plotted as $\beta\gamma = (1/c)(p_P/M_P)$ vs plate number.

[12] The effect of air gaps is taken into account in the density correction in Appendix E.
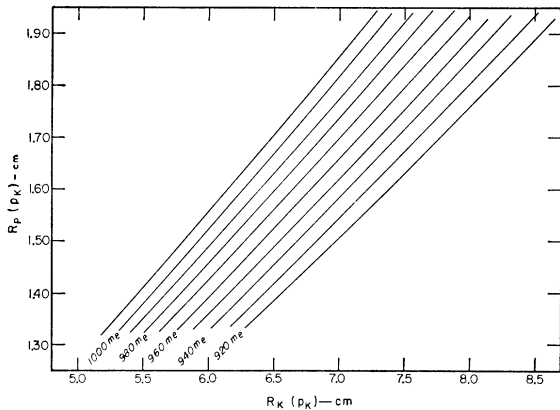
FIG. 7. Curves giving $R_K(M_K,p_K)$ vs $R_P(M_P,p_K)$ for various values of M_K.

Each track was followed to as near the edge of the emulsion as possible in order to establish its entrance position for the momentum determination. When a track was lost in the densely populated region of the protons, the entrance point was estimated by assuming that the track went half the remaining distance to the edge, maintaining the direction when last seen, and then followed the average particle direction for that plate as determined from the protons. An error of one plate in the entrance position would have resulted in an individual mass error of 1.5 m_e. Most estimates should have erred randomly by less than half a plate, or 0.8 m_e.

G. Evaluation of the Masses

The range $R_K(p_K)$ of a particle of charge Z_K, mass M_K, and momentum p_K can be expressed in terms of the known range $R_P(p_P)$ of a particle of charge Z_P, mass M_P, and momentum p_P as

$$R_K(p_K) = \left(\frac{Z_P}{Z_K}\right)^2 \frac{M_K}{M_P} R_P\left(\frac{M_P}{M_K} p_K\right). \qquad (1)$$

This equation forms the basis of the momentum-range method. The mass M_K is thus determined from a knowledge of Z_K, Z_P, M_P, and the range-momentum relation $R_P(p)$ of the reference particle over the momentum regions $(M_K/M_P)p_K$ and p_K. The latter region is concerned in the determination of the momentum p_K as indicated in Sec. IIC. In this experiment $Z_K = Z_P = 1$, the proton mass M_P was taken to be 1836.1 m_e, and $R_P(p)$ was taken from the proton range tables of Barkas and Young[13] and the recent values of Barkas, Heckman, and Smith[14] (see Appendix E, 2).

By means of Eq. (1) and the proton range-momentum

---

[13] W. H. Barkas and D. M. Young, University of California Radiation Laboratory Report UCRL-2579 (Rev.), September, 1954 (unpublished).

[14] Barkas, Heckman, and Smith, University of California Radiation Laboratory Report UCRL-3298 (Abstract), February, 1956 (unpublished).

relations, it was possible to construct a family of isomass curves by plotting, for various masses, the meson range $R_K(p_K)$ as a function of the proton range for the same momentum, $R_P(p_K)$. A small-scale reproduction is shown in Fig. 7. Each event was recorded as a point on the graph with coordinates (R_K,R_P), using the measured value of R_K and the value $R_P = R_{0P}(p_{0K})$ appropriate to the meson's entrance position as described in Sec. IIC2. The corresponding mass was obtained by interpolating between the two nearest isomass lines. The masses were estimable to 0.5 m_e, but actually the nearest integral value was used.

III. EXPERIMENTAL RESULTS

A. Characteristics of the Mass Distributions

Histograms showing the actual distributions of the $K_{\pi3} = \tau + \tau'$, $K_{\pi2}$, and $K_{\mu2}$ masses are presented in Fig. 8. The results of an examination of these distributions are found in Table II. In each group were a few abnormally high mass values. These probably resulted from collisions with the magnet pole piece or from inelastic scatters in the emulsion, which would have shortened the range and thus increased the apparent mass (see Appendix E, 5). In order to obtain the most valid average of the masses, these events were eliminated on the basis of Chauvenet's Criterion.[15] It is of some interest that the relative number of events in this category was about the same for all decay modes. As distributions were nearly Gaussian, no great error should have resulted from the assignment of the mass cut-off values on the basis of the normal probability
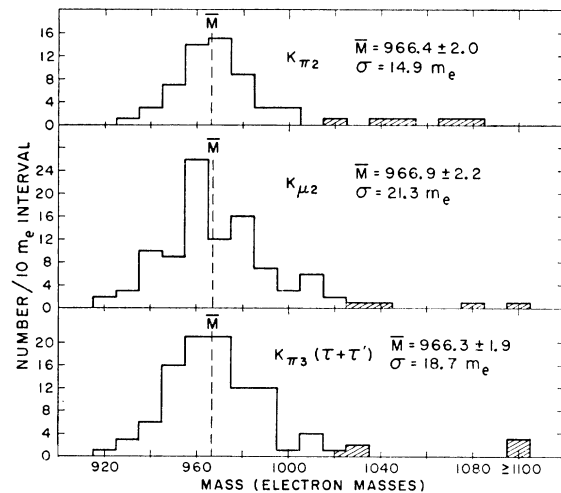
FIG. 8. Histograms showing the $\tau + \tau'$, $K_{\pi2}$, and $K_{\mu2}$ mass distributions. The shaded events were eliminated from the mass averages by Chauvenet's criterion.

---

[15] Chauvenet's Criterion eliminates events from a sample of size n, where the probability is less than $\frac{1}{2}n$ that the event in question is a part of the distribution. See, for instance, Y. Beers, *Introduction to the Theory of Error* (Addison-Wesley Press, Cambridge, 1953), p. 23.

TABLE II. Characteristics of the main mass distributions. (All mass quantities are in units of the electron mass.)

Particle	$K_{\pi 3}$	$K_{\pi 2}$	$K_{\mu 2}$
Total No. measured	104	60	100
Number accepted in averaging	98	54	96
Mean mass	966.3	966.4	966.9
Standard error	±1.9	±2.0	±2.2
Standard deviation σ	18.7	14.9	21.3
Chauvenet's ($\Delta M_{\max}/\sigma$)	2.79	2.60	2.79
Chauvenet's cutoff	1017.7	1005.2	1026.5
Nearest excluded mass M_x	1021	1017	1027
$\Delta M_x/\sigma$	2.90	3.40	2.82
Alternate mean mass[a]	966.8	967.4	967.5
Alternate std. error[a]	±1.9	±2.2	±2.2
Alternate std. dev. σ'[a]	19.3	16.3	21.8
Alternate $\Delta'M_x/\sigma'$	2.80	3.05	2.73

[a] The alternate values include excluded mass M_x nearest the cutoff.

distribution and the standard deviations of the individual distributions. As a check, the averages and standard deviations were computed for the mass distributions modified by the inclusion of the excluded value nearest the cutoff. These results are also given in Table II.

B. Predicted Mass Distribution

For a test of the reasonableness of the experimental mass distribution, it was possible to construct a distribution curve predicted from the expected behavior of the variables influencing the measurement. It was necessary to consider the effects of range straggling and the momentum distribution characterizing each entrance point in the following way.

In the velocity region of the K mesons, the mean range R' of a particle of mass M_0 and momentum p behaves as $R'/M_0 = C_1(p/M_0)^{3.0}$, where C_1 is constant. A measure M of the mass M_0 based on the known momentum p and the actual range R will not in general yield the true mass $M = M_0$ because of the range straggling of R about R'. In fact, the measured value M will follow the relation $M = C_2 R^{-1.5} p^{1.5}$. We define R_0 by the equation

$$M_0 = C_2 R_0^{-0.5} p_0^{1.5},$$

where $p_0(y)$ is the average momentum of all particles of the same entrance position y. The true momentum p varies about p_0 because of the finite target width (Appendix D). From these relations, it follows that the mass value M obtained by using the measured range R and the mean momentum $p_0(y)$ can be expressed as

$$\frac{M}{M_0} = \left(\frac{R}{R_0(y)}\right)^{-0.5}\left(\frac{p}{p_0(y)}\right)^{1.5}. \qquad (2)$$

We make the reasonable assumption that the relative rms range straggle $\sigma_{R(y)}/R_0(y)$ was constant across the stack, as was the relative momentum standard deviation $\sigma_{p(y)}/p(y)$. From the average standard devia-

tion $\sigma_M = 19.1\ m_e$ actually obtained from the mass distributions, we find in Appendix D that $\sigma_p/p = 0.012$ for the calculated value of $\sigma_R/R = 0.016$.

We can now obtain a plot of the relative mass distribution function $P(M/M_0)$ by graphical methods. We first construct a curve defining the distribution $P(R/R_0)$ by using the relation $R'/R_0 = (p/p_0)^{3.0}$ and a plot of the Gaussian distribution $P(p/p_0)$ of standard deviation 0.012, weighted according to $d(R'/R_0)/d(p/p_0)$. Next, the distribution $P(R/R_0)$ is obtained by folding into $P(R'/R_0)$ the straggling distribution $P(R/R')$, a Gaussian of the calculated standard deviation 0.016. Finally, the function $P(M/M_0)$ can be plotted by using the relation $M/M_0 = (R/R_0)^{-0.5}$ and the distribution $P(R/R_0)$ weighted according to $d(M/M_0)/d(R/R_0)$. From $P(M/M_0)$ the distribution function $P(M)$ was obtained by using $M_0 = 966.5\ m_e$, and a normalized curve of this predicted distribution was plotted along with a histogram of all events combined; the result is shown in Fig. 9. The fit is surprisingly good. Deviations from a Gaussian are greatest in the high-mass tail, but can be noticed in the peak as well. The total effect of these deviations is not large; nevertheless the skewness is apparent and its result on the mass average is discussed below in Appendix E. The curve also demonstrates the validity of the mass cutoff used in the averaging.

C. Average Masses

In Table III are presented the averages of the masses obtained from the measurements, the errors, and certain small corrections that are discussed in Appendix E along with the systematic uncertainties. Also listed are the values and standard errors of the mass differences $M_K - M_\tau$ and $M_K - M_{(\tau+\tau')}$. The standard errors are based on the standard deviations of the individual distributions, except for those of the $K_{\mu 3}$ and $K_{\beta 3}$, whose small number of events made it more reasonable to use the average standard deviation of the other distributions.

The average mass values and standard errors are such that any mass differences existing among the τ, $K_{\pi 2}$, and $K_{\mu 2}$ mesons are less than $3\ m_e$ with a probability of 70%, and that the $K_{\mu 3}$ and $K_{\beta 3}$ masses are similarly equal to the others to within $5\ m_e$ and $8\ m_e$, respectively. These results are in agreement with other
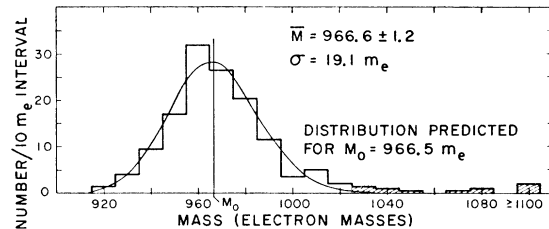
FIG. 9. Histogram of the masses of all decay modes combined, and the predicted mass distribution (normalized). The shaded events were eliminated from the mass average.

TABLE III. Values of the average masses and corrections. (All quantities pertaining
to the mass are in units of the electron mass m_e.)

Particle type	τ	τ'	$\tau+\tau'$	$K_{\pi 2}$	$K_{\mu 2}$	$K_{\mu 3}$	$K_{\beta 3}$	All
Mean measured mass	966.0	967.4	966.3	966.6	966.9	969	967	966.7
Standard error (m_e)	±2.1	±4	±1.9	±2.0	±2.2	±5	±8	±1.1
Estimated systematic error	±1.6	±1.6	±1.6	±1.6	±1.6	±1.6	±1.6	±1.6
Number of events used	77	21	98	55	96	12	6	267
Averaging correction[a]	−0.3±0.1	−0.3±0.1	−0.3±0.1	−0.3±0.1	−0.3±0.1	−0.3±0.1	−0.3±0.1	−0.3±0.1
Range-momentum correction[a]	+0.7±0.5	+0.7±0.5	+0.7±0.5	+0.7±0.5	+0.7±0.5	+0.7±0.5	+0.7±0.5	+0.7±0.5
Emulsion density correction[a]	+0.4±0.1	+0.4±0.1	+0.4±0.1	+0.4±0.1	+0.4±0.1	+0.4±0.1	+0.4±0.1	+0.4±0.1
Inelastic events correction[a]	−0.5±0.5	−0.5±0.5	−0.5±0.5	−0.5±0.5	−0.5±0.5	−0.5±0.5	−0.5±0.5	−0.5±0.5
Corrected absolute mass	966.3	967.7	966.6	966.9	967.2	969	967	967.0
Combined statistical and systematic uncertainty on absolute mass	±2.7	±4.3	±2.6	±2.7	±2.8	±5	±8	±2.1
M_K-M_τ (standard errors)		1.4±4.5		0.6±2.9	0.9±3.0	1.3±5	−2.7±8	
$M_K-M_{\tau+\tau'}$ (standard errors)				0.3±2.8	0.6±3.0	1.0±5	−3.0±8	

[a] See Appendix E.

recent relative mass measurements[8,16,17] and are improved by a twofold reduction in the standard errors. In addition, an evaluation of the meson masses relative to the proton mass indicates that the primary mass values are equal to those obtained from Q-value determinations[11] to within the experimental errors of about $3\ m_e$.

D. Significance of the Results

The results indicate at least a very near degeneracy among the K-meson masses regardless of the associated decay modes. Less than two years ago this fact would have been exciting if not startling; however, in the past year, there has been a general trend toward an acceptance of the idea, and in recent months some theoretical attempts have been made to reconcile this degeneracy with the increasingly apparent difference between the spin-parity configurations of the τ $(0, -)$[10,18] and $K_{\pi 2}$ $(0, +)$.[19] It has also been established that, at least for the particles that come to rest in the order of 10^{-8} sec,[20] the τ, $K_{\mu 2}$, and $K_{\pi 2}$ all have very nearly the same mean life.[21]

Lee and Orear[1] propose a scheme wherein there are two primary heavy mesons, the θ and the τ, the heavier of which is capable of decaying via γ decay into the lighter, which has a different spin-parity configuration. The lifetime of the heavier corresponds to the measured value of about 10^{-8} sec, and the lighter (daughter) decays in a time short compared to 10^{-8} sec, so that its

measured lifetime is the same as the parent's if the measurement is made on stopped particles. Either or both the τ and θ may contribute to the $K_{\mu 2}$, $K_{\mu 3}$, and $K_{\beta 3}$. Thus, if this scheme is correct, the primaries of all decay modes in this experiment are the same particle (hence no primary mass differences). However, the masses based on the Q-value determinations should differ between the θ and τ, unless the transition energy between the two states is too small to be detectable as a mass difference. Several variations of the scheme are possible. Accurate Q-value determinations of the $K_{\pi 2}$ and $K_{\mu 2}$ masses as well as of the τ mass are obviously important as a means of evaluating the validity of this cascade concept of K-meson behavior. It might be mentioned that the recoil from the decay of a K particle at rest into a γ ray and another K particle would have been too short for identification as such unless the energy transition were greater than about 15 Mev (recoil of 3 microns). Q-value mass measurements[11] dictate that any transition must be an order of magnitude smaller, and hence the recoil would not have been detected.

Lee and Yang[22] and Gell-Mann[23] have recently suggested that the apparent $\theta-\tau$ mass degeneracy actually follows from an invariance law. They assume that the τ and θ have identical spin (0)[19] but opposite parity, and propose a new "parity conjugation" operator that changes the τ of minus parity into a θ of plus parity, and vice versa. The identity or near identity of the τ and θ masses results from conservation of parity conjugation by strong interactions. Gell-Mann believes that parity conjugation is conserved by electromagnetic as well as strong interactions, and that the conservation fails only in weak (leptonic) interactions, hence the mass difference should be only a small fraction of an electron mass. One would expect rather long $(\sim 10^{-8}$ sec$)$ but not identical lifetimes. On the other hand, Lee and Yang admit the possibility of a violation of the con-

[16] Ritson, Pevsner, Fung, Widgoff, Zorn, Goldhaber, and Goldhaber, Phys. Rev. 101, 1085 (1956).

[17] Heckman, Smith, and Barkas, Nuovo cimento 3, 85 (1956).

[18] Orear, Harris, and Taylor, Phys. Rev. 102, 1676 (1956).

[19] Evidence of the $\theta^0 \to 2\pi^0$ decay, hence even-integer spin of the θ^0, has been found by J. Osher, University of California Radiation Laboratory Report UCRL-3449, June, 1956 (unpublished). Spin zero is more naturally favored than a spin two or greater.

[20] The proper time of flight of the K mesons in this experiment was 1.4×10^{-8} sec.

[21] V. Fitch and R. Motley, Phys. Rev. 101, 496 (1956); R. Motley and V. Fitch, Phys. Rev. 105, 265 (1957); Alvarez, Crawford, Good, and Stevenson, Phys. Rev. 101, 503 (1956), and to be published.

[22] T. D. Lee and C. N. Yang, Phys. Rev. 102, 290 (1956).

[23] M. Gell-Mann (private communication).

servation of parity conjugation in electromagnetic interactions, and thus the existence of a mass difference between the θ^+ and τ^+ of the same order of magnitude at that between the π^0 and $\pi^\pm$, or smaller, which could be compatible with the Lee-Orear scheme. A spin $0-0$ transition requires the emission of at least two γ's, and a mass difference should be of the order of 10 Mev[7] (thus measurable) for a lifetime of about 10^{-8} sec.

From the results of this experiment alone one can make no choice between these ideas; the data simply indicate that the particles passing through the system, with lifetimes of at least 10^{-8} sec, have close to the same mass. A genetic relationship as per Lee and Orear is, in principle, allowed by these data; however, the Q-value measurements require θ, τ mass difference in this scheme to be less than about 2 or 3 Mev.[11] The "parity conjugation" ideas are agreeable with existing data, with the stipulation that the measured stopped-particle lifetimes are the same[21] and that, from this experiment, if the actual lifetimes are the same, any mass difference is no greater than about 1 Mev, for if the lifetimes are equal we have indeed measured the masses of the actual parents to the decay products.

ACKNOWLEDGMENTS

APPENDIX A. SHORTENING OF THE PROJECTED PROTON RANGE DUE TO MULTIPLE SCATTERING IN THE EMULSION

The range-energy relation deals with the average range $\langle R \rangle_{Av}$ along the track and includes the effect of range straggling.

The difference between the actual total length of track R_0 and its projection R_{0x} along an axis representing the initial direction of the particle is

$$R_0 - R_{0x} = \int_0^{R_0} (1 - \cos\theta)dR, \qquad (3)$$

where θ is the spatial angle between the actual path and the initial direction. For small angles we use the approximation $\cos\theta = 1 - \frac{1}{2}\theta^2$. The average shortening of a large number of tracks of equal initial energy is

$$\langle R_0 - R_{0x} \rangle_{Av} = \int_0^{R_0} \left(\frac{\theta^2(R)}{2} \right)_{Av} dR,$$

and, as the distribution in θ is Gaussian, we have

$$\langle R_0 - R_{0x} \rangle_{Av} = \int_0^{R_0} \frac{\theta_{rms}^2(R)}{2} dR. \qquad (4)$$

The range shortening is calculated in terms of the root-mean-square multiple-scattering angle (a function of the range).

In order to most satisfactorily describe the scattering in photographic emulsion, we choose to use an expression basically derived from theory but fitted to experimental data on multiple scattering in emulsion. This function evaluates the mean absolute *projected* angle between two successive chords connecting points at intervals Δt along the path. We shall refer to this angle as $\Delta\theta_{x\,chord}$, and when expressed in radians it has the average value[24]

$$\langle \Delta\theta_{x\,chord} \rangle_{Av} = \frac{\pi}{180} \frac{K}{pv} \left(\frac{\Delta t}{100} \right)^{\frac{1}{2}} \text{radians}, \qquad (5)$$

for a singly charged particle of momentum $p(\text{Mev}/c)$ and velocity $v(\text{cm/sec})$, when measured over a length $\Delta t(\text{microns})$. The "scattering constant" $K(\text{degrees} \times \text{Mev}/100 \text{ microns})$ is determined empirically for a particular type of emulsion, and is a slowly varying function of velocity and the cell length Δt.

The relation between $\langle \Delta\theta_{x\,chord} \rangle_{Av}$ in (5) and the *spatial* angle $\Delta\theta$ between successive tangents to the path used in (4) can be shown to be

$$\Delta\theta_{rms} = (3\pi/2)^{\frac{1}{2}} \langle \Delta\theta_{x\,chord} \rangle_{Av}.[25]$$

Using the nonrelativistic relation $pv = 2T$ and the ap-

[24] Gottstein, Menon, Mulvey, O'Ceallaigh, and Rochat, Phil. Mag. 42, 708 (1951).
[25] J. R. Peterson, University of California Radiation Laboratory. Report UCRL-3284, April, 1956 (unpublished).

proximate range-energy relation

$$T = AR^\eta m^{1-\eta}, \tag{6}$$

we obtain

$$\Delta\theta_{\mathrm{rms}}{}^2 = \frac{3\pi}{8A^2}\left(\frac{\pi}{180}\right)^2 KR^{-2\eta}m^{-2(1-\eta)}\left(\frac{\Delta t}{100}\right) \tag{7}$$

for a particle of *residual* range R(microns), mass m in units of the proton mass, and kinetic energy T(Mev). $\Delta\theta$ is in radians.

A large number of particles, initially traveling in the same direction with residual range R_0, will, after reaching a point with residual range R, exhibit a mean-square angular deflection that may be expressed as

$$\theta_{\mathrm{rms}}{}^2 = \int_{R_0}^{R} \frac{d\theta_{\mathrm{rms}}{}^2}{dR} dR. \tag{8}$$

We let $\Delta t \rightarrow -dR$ in Eq. (7) (the minus sign derives from the fact that R is measured backwards from the end of the range), and $\Delta\theta_{\mathrm{rms}}{}^2 \rightarrow d\theta_{\mathrm{rms}}{}^2$, then Eq. (8) becomes, upon integration:

$$\theta_{\mathrm{rms}}{}^2 = 10^{-2}\left(\frac{\pi}{180}\right)^2 \frac{K^2 m^{-2(1-\eta)}}{A^2(1-2\eta)}(R_0^{1-2\eta} - R^{1-2\eta}). \tag{9}$$

The evaluation of Eq. (4), with the use of Eqs. (9) and (6), yields the desired expression for the average range shortening for protons of initial range R_0 (microns) and kinetic energy T_0(Mev):

$$\langle R_0 - R_{0x}\rangle_{\mathrm{Av}} = 10^{-2}\left(\frac{\pi}{180}\right)^2\left(\frac{3\pi}{16}\right)\frac{K^2}{2(1-\eta)}\left(\frac{R_0}{T_0}\right)^2. \tag{10}$$

Taking the value of $K = 27$ (degrees$\times$Mev/100 microns) from Menon's data[24] as a suitable average over the ranges considered, and an average $\eta = 0.57$ from Barkas,[13] we obtain the final result:

$$\langle R_0 - R_{0x}\rangle_{\mathrm{Av}} = 1.53\times10^{-3}(R_0/T_0)^2. \tag{11}$$

These corrections amounted to roughly 0.5% of the proton ranges. The proton tracks had a mean absolute angular deviation of less than 20° to within 20 μ of the end, justifying the small angle approximation. The approximation $pv = 2T$ holds for 65-Mev protons, but the assumed constant values of η and K may have caused an error, probably less than 15% of the total correction, or 0.075% of the range. The result would have been an error in momentum of 0.022% or 0.03% in meson mass. Any systematic mass error incurred in this correction, then, was probably less than 0.3 m_e.

APPENDIX B. CORRECTION FOR NONNORMAL ANGLES OF INCIDENCE

As described briefly in Sec. IIC, the average incident angle varied according to the entrance position. The resulting dip of the track caused a shortening of the
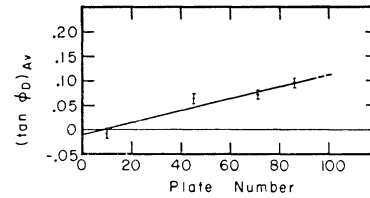
FIG. 10. The tangent of the incident dip angle ϕ_D vs plate number.

projected proton ranges and also meant that the entrance plate was not that in which the ranges were measured. The average tangent of the dip angle ϕ_D that a track makes with the emulsion plane was determined in four different plates across the stack. These averages were plotted as shown in Fig. 10, and a straight line was drawn to approximate a fit. The measured proton ranges were then modified and the appropriate entrance plate was chosen on the basis of the values of $\tan\phi$, taken from the curve.

The average of the tangent was taken from the measurements on a group of individual proton tracks selected in a systematic manner to avoid any bias. In each emulsion, these tracks were followed from about 3 mm from the edge of the emulsion until they either left the plate or had traveled about 2 mm. The depth of the track in the emulsion was recorded at each end point and the difference was increased by the factor 2.5 to compensate for shrinkage during development. It was also necessary to correct the measured distance between the end points on all diving tracks because of a distortion of the original y-z plane (parallel to the face of the stack) in each emulsion as shown in Fig. 11. This distortion resulted from an inward shift of the bulk of the emulsion during development, while the bottom (glass) surface remained fixed. It can be seen that the uppermost 40 μ of the emulsion was left relatively undistorted, the shift having been equal for all depths in this region. The effect was greatest at the edge of the emulsion, decreasing to zero at about 10 mm from the
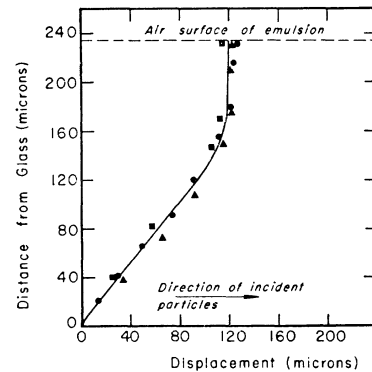
FIG. 11. The typical lateral (inward) shift of the emulsion after development, measured about 3 mm from the leading edge of one of the plates. Experimental points taken from measurements on three different tracks are shown. Direction of the incident particles in the emulsion is indicated.

edge. The character and magnitude of the shift appropriate to the dip angle measurements were determined by examining steeply diving tracks in the region of the measurements. The original direction of a track was established in the undistorted upper region of the emulsion and the relative distortion of the emulsion below was ascertained from the measured displacement of the actual track from the projection of the undistorted track at various depths. A curve similar to Fig. 11 was constructed for each plate in which the dip angles were measured. It can be seen that for diving tracks this distortion would effectively increase the dip that had characterized the track in the unprocessed emulsion.

APPENDIX C. CORRECTION FOR MOMENTUM LOSS IN AIR

The fact that protons and mesons of equal momentum have different rates of loss of energy and momentum in matter assumed significance in the air path following the onset of the momentum analysis, and resulted in a difference in the momenta of the mesons and protons of the same entrance position. A correction for the effect was made by computing this difference and shifting the proton range curve (Fig. 4) laterally in the y direction a distance dictated by the momentum dispersion dp/dy so that the new range corresponded to a proton momentum identical to that of the K's for the same entrance y. Several values of dp/dy were obtained by graphically differentiating the (proton) momentum curve (Fig. 5) and from these values a curve (Fig. 12) was constructed to represent dp/dy as a function of the entrance plate.

In the correction, it was necessary to consider the paths between the entrance to the magnet and the emulsion stack (see Fig. 2). An exact analytical treatment would have been very difficult because of complexities arising from the action of the magnetic field and the geometry of the system. The help of several justifiable approximations, however, made possible a relatively simple yet quite accurate semianalytic procedure.

Since the total change in momentum, and hence in radius of curvature along the air path in the magnet, was only about 0.7% for the protons and 0.2% for the mesons, we can restrict the approximation to the first order in small quantities. The rate of change of momentum, dp/dx, can be treated as a constant over the air path, its magnitude depending on the particle type and initial momentum p_0.

$$dp/dx = -k_1(p_0). \tag{12}$$

While in the magnetic field B, the particle trajectory has a radius of curvature

$$\rho = (3.336pc/BZ) \text{ cm}, \tag{13}$$

where pc is in Mev, B is in kilogauss, and the net charge Z on the particle is in electronic charge units
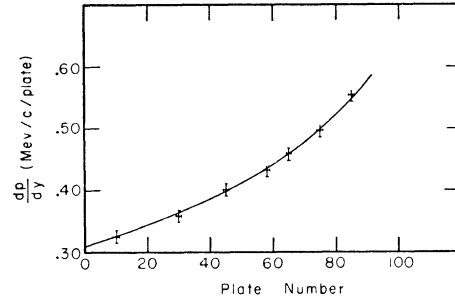
FIG. 12. The momentum dispersion dp/dy according to the entrance plate number.

($Z=1$ here). Assuming B is constant, we have ρ equal to a constant times the momentum:

$$\rho = k_2 p, \tag{14}$$

and hence

$$dp/dx = -k_1 k_2.$$

If ϕ represents the angle through which the trajectory turns in a path length x, and if $\phi = 0$ at the entrance to the magnet, then at any value of ϕ, we have

$$dx(\phi) = \rho d\phi$$
$$= [\rho_0 + (d\rho/d\phi)\phi]d\phi.$$

Since $(d\rho/d\phi)\phi_{total}$ is less than $0.01\rho_0$, we obtain

$$dx \simeq \rho_0 d\phi, \tag{15}$$

and thus

$$dp = -k_1 k_2 \rho_0 d\phi = -k_3 d\phi. \tag{16}$$

The trajectory of a particle in the magnet, then, can be well approximated by the involute of an inextensible string of initial length ρ_0 winding around a cylinder of radius $k_3 = k_1 k_2 \rho_0$, as shown in Fig. 13, with k_3 exaggerated relative to the other dimensions ($k_3 \simeq 10^{-2}\rho_0$). The locus of the center of curvature is actually a spiral, but the error caused by the circle approximation is very small ($\sim 3\%$ of the correction).

Referring to Fig. 13, we note that, at the exit from the magnet, the lateral separation Δy_m between a
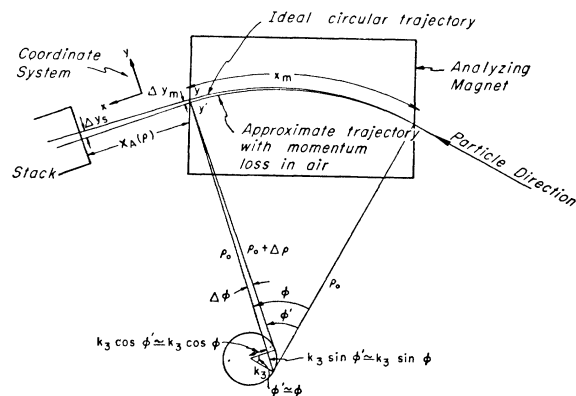
FIG. 13. Diagram used in obtaining the correction for the momentum loss in air.

truly circular trajectory and the "actual" trajectory can be expressed as

$$\Delta y_m = {}_m' - y_m = \rho_0 + \Delta\rho + k_3\sin\phi - \rho_0$$
$$= \Delta\rho + k_3\sin\phi,$$

and using Eq. (16), we have

$$\Delta y_m = -k_3(\phi - \sin\phi). \tag{17}$$

The angle $\Delta\phi$ between the two trajectories is

$$\Delta\phi = \phi' - \phi \cong (k_3/\rho_0)(1 - \cos\phi). \tag{18}$$

If the path length between the magnet and the stack is $x_A(\rho_0)$, the difference in y at the stack is

$$\Delta y_s = y_s' - y_s$$
$$= y_m' - y_m - x_A\sin\Delta\phi \cong \Delta y_m - x_A\Delta\phi$$
$$= -k_3[(\phi - \sin\phi) + (x_A/\rho_0)(1 - \cos\phi)]$$
$$= \frac{d\rho}{dp}\frac{dp}{dx}[\rho_0(\phi - \sin\phi) + x_A(1 - \cos\phi)]. \tag{19}$$

We designate the path length in the magnet as $x_m(\rho_0)$. The total path in air, x_T, after momentum analysis begins, is $x_T = x_m + x_A$, and we assume that these distances are the same for both mesons and protons of the same momentum. We now assign the subscripts K and P to all functions representing mesons and protons when these functions are significantly different for the two cases. If the momentum dispersion at the magnet is dp/dy (slowly varying function of y), then the difference Δp_s in the momentum between the protons and mesons at the entrance to the stack for any value of y is

$$\Delta p_s(y) = (p_K - p_P)_s$$
$$= \left(\frac{dp_K}{dx} - \frac{dp_P}{dx}\right)x_T$$
$$+ \frac{dp}{dy}[-(y_s' - y_s)_K + (y_s' - y_s)_P]$$
$$= \left(\frac{dp_K}{dx} - \frac{dp_P}{dx}\right)\left\{x_T - \frac{d\rho_0}{dp}\frac{dp}{dy}\right.$$
$$\left. \times[\rho_0(\phi - \sin\phi) + x_A(1 - \cos\phi)]\right\}. \tag{20}$$

The value of Δp was computed for three different values of y. The proton momenta appropriate to these points were obtained from Fig. 5, and dp/dy from Fig. 13. The remaining quantities in Eq. (20) were determined for each point as follows:

1. $dp/dx = (1/\beta c)(dT/dx)$: values of dT/dx in air for both the protons and mesons were obtained from the

range-energy tables (for protons) of Rich and Madey.[26] Appropriate numbers in the table were modified to hold for the mesons. The air density was taken equal to 1.19×10^{-3} g/cm^3($23°$C).

2. ρ_0 and $d\rho_0/dp$ were determined by using the measured values of p and B ($=9.25$ kilogauss) in Eq. (13).

3. $\phi(\rho_0)$ was extracted from the original wire-trajectory data.

4. In order to include the effect of the fringe field, x_m was taken to be equal to $\rho_0\phi$ rather than $x_{m\,(\text{geom})}$, the length predicted by ρ_0, by the angle of incidence at the magnet, and by the magnet dimensions.

5. x_A, the magnetic-field-free path length was taken to be the physical distance from the stack to the magnet for a particular ρ_0, less the effective extent of the fringe field as estimated from $\frac{1}{2}[x_m - x_{m\,(\text{geom})}]$ (factor $\frac{1}{2}$ so as to include only the exit edge).

Knowing the momentum difference Δp between the mesons and the protons, one could calculate the distance Δy by which the proton range curve should be shifted so as to accurately represent the true meson momentum. The expression

$$\Delta y = -\Delta p/(dp/dy) \quad (\text{function of } y)$$

was used in computing the shift for each of the three points. A smooth curve $\Delta y(y)$ was then constructed to fit the points, and the proton range curve was changed accordingly. It was then possible to compute the masses as described in Sec. IIG.

This correction effectively increased the K mass values by an amount varying from $6.3\,m_e$ at the high-momentum side to $8.5\,m_e$ for the low momenta. The calculation should have been good to about 20%, or $1.5\,m_e$.

APPENDIX D. DISCUSSION OF THE STATISTICAL ERRORS

Deviations of the individual mass values from the means were due largely to the spread in momentum characterizing any point at the face of the stack, and the range straggling of the K mesons. To a much lesser extent the precision of measurement was also affected by the uncertainty in determining the entrance position of a particular meson and by errors in measuring the true ranges of the mesons and the protons.

The incident K mesons were in a velocity region such that the range-momentum relationship could be expressed by

$$R/M = C_1(p/M)^{3.0}, \tag{21}$$

hence

$$M = C_2(R)^{-0.5}(p)^{1.5}, \tag{22}$$

where C_1 and C_2 are constants.

The percentage straggling can be considered independent of momentum over the small momentum in-

[26] M. Rich and R. Madey, University of California Radiation Laboratory Report UCRL-2301, March, 1954 (unpublished).

terval existing at each entrance position. Thus we can consider, as contributing to the variations of M about the actual mass M_0, the independent variations of R, due to straggling, about $R_0(y)$ and p about $p_0(y)$. R_0 is defined (Sec. IIIA1) by $M_0 = C_2 R_0^{-0.5} p_0^{1.5}$ where $p_0(y)$ is the mean momentum of particles entering the stack at a given position y. We assume that the relative standard deviations σ_R/R_0 and σ_p/p_0 were constant across the stack. The root-mean-square deviations are related according to

$$\frac{\sigma_M}{M_0} = \left[\left(0.5\frac{\sigma_R}{R_0}\right)^2 + \left(1.5\frac{\sigma_p}{p_0}\right)^2\right]^{\frac{1}{2}}. \quad (23)$$

The dominant contribution to σ_R/R_0 was the K-meson range straggling of 1.6%. The errors in measurement of the meson range were less than 0.2% and could be neglected in σ_R compared to the straggling, since each type of error enters the total in quadrature.

The total $\sigma_p/p_0 = 1.2\%$ was obtained from Eq. (23) by use of the observed value of $\sigma_M/M_0 = 1.9\%$ and the calculated $\sigma_R/R_0 = 1.6\%$. The errors in momentum deriving from inaccuracies in estimating the entrance position (0.1%) and in ascertaining the true mean proton range (0.2%) were an order of magnitude smaller than the total, and thus were negligible compared to the spread in incident momentum at each point on the face of the emulsion stack. This momentum spread was due mainly to the multiple scattering in the 0.09-inch Al window in the Bevatron vacuum tank and to a smaller extent to the finite size of the target and the multiple scattering in the air. The effect of the scattering in such a system is to give an apparently finite width to a line target, resulting in an apparent target that varies in density according to a Gaussian distribution.

In this experiment the scattering was such as to produce a 1.2-inch width for a line target for the protons and a 0.63-in. width for the mesons, where the width represents twice the standard deviation on the Gaussian. The actual target was 0.625 in. wide, and when the effect of the scattering was folded into this square distribution, there resulted apparent targets that were in both cases almost Gaussian and had widths of 1.2 in. (protons) and 0.70 in (mesons).

The resulting magnitude of the relative spread in momentum may be estimated by the equation

$$\frac{dp}{p} = \frac{1}{p}\frac{dp}{dy}M_H L_H, \quad (24)$$

where dp/dy is the change in momentum per cm across the stack, M_H the horizontal magnification of the lens system, and L_H the effective width of the target. The quantities p and dp/dy were found (from the proton ranges) to be about 360 Mev/c and 6.6 (Mev/c)/cm. The magnification was estimated from the wire measurements with an accuracy of about 30% to be about 0.6×.

These values and those above for the estimated effective target size yield momentum spreads of 0.9% for the mesons, to be compared with the value 1.2% deduced from the mass distribution, and 1.6% for the protons, compared to 1.9% deduced from the proton range distribution. The magnitude of the increase in the momentum uncertainty due to scattering in the air was not calculated. However, a simple estimate indicated that the effect was no more than one-third as large as that caused by the scattering in the aluminum window. It is probable, then, that the slight disagreement between the predicted and deduced momentum spreads is due to the air-scattering. In general the agreement is very good, considering the uncertainty in the horizontal magnification.

APPENDIX E. DISCUSSION OF POSSIBLE SYSTEMATIC ERRORS AND SOME SMALL CORRECTIONS AFFECTING THE ABSOLUTE MASS VALUES

The results may have been affected by certain systematic errors other than those corrected for in Appendices A, B, and C. Some of the effects indicated below may be more properly classed as corrections than errors, and some possess the properties of both. It is to be noticed that in any case these errors apply to the absolute mass values alone; the values of the masses relative to each other are affected by only the nonsystematic errors discussed above unless there exist differences in energy-loss processes among the various types. The effects treated in the Appendices A, B, and C would have given slightly greater spreads to the mass distributions, as well as systematic deviations of the averages had they not been considered.

Systematic errors may have resulted from:

1. Errors in the various corrections considered in appendices above. The magnitudes of these errors are estimated at the end of each Appendix and they affect the absolute mass as follows:

Error in range-shortening correction $\sim 0.3\ m_e$,
Error in entrance-angle correction $\sim 0.4\ m_e$,
Error in effect-of-air correction $\sim 1.5\ m_e$.

We shall assume that these are randomly distributed and may be added in quadrature. Then the total uncertainty of these corrections should have been less than 1.6 m_e.

2. Errors in the range-momentum relations. The masses were determined on the basis of Eq. (1) rewritten as

$$M_K = M_P R_K(p_K) \bigg/ \left[R_P\left(\frac{M_K}{M_P}p_K\right)\right], \quad (25)$$

where $R_K(p_K)$ is the measured range of a meson of momentum p_K, and R_P is the proton range for momentum $(M_P/M_K)p_K$. The momentum p_K was obtained from the tables of Barkas and Young,[13] for the proton

range $R_P(p_K)$ from Fig. 5. Thus, the mass determination involves the two different momentum regions p_K and $(M_P/M_K)p_K$. In the region of p_K, the proton range R_1 follows the approximation $R_1 = K_1 p_K^{3.35}$, and in the region of $p_2 = (M_P/M_K)p_K$ it obeys Eq. (21): $R_2 = K_2 p_2^{3.0}$. It can be shown that if the ranges R_1 and R_2 should be increased by ΔR_1 and ΔR_2, respectively, in order to correct errors in the range-momentum relations, then the mass values obtained in the experiment should be corrected by adding

$$\Delta M = \left(\frac{\Delta R_2}{R_2} - \frac{3.0}{3.35} \frac{\Delta R_1}{R_1} \right) M \qquad (26)$$

to the measured values. The range curves used were compared with the range tables recently recalculated by Barkas.[13] The curve expressing $R_1(p_1)$ was found to agree almost exactly with the new values, but the values for $R_2(p_2)$ were slightly lower than the revised points in the upper third of the momentum region concerned, the maximum error being about 0.55% in R_2. It was estimated, by examining the particles' range-distribution, that one third of the mass values should be increased by $2\ m_e$, thus a total correction of $0.7\ m_e$ on all mass values should be made if the new range values are correct.

An error in the value of the mean ionization potential used $(323\pm11\ \text{ev})$[13] is reflected in a constant percentage error in the momentum deduced from any range, according to Barkas.[27] Equation (26) may be rewritten as

$$\Delta M = 3.0(\Delta p_2/p_2 - \Delta p_1/p_1)M.$$

Thus if the percentage error in the momentum is constant owing to an error in the mean ionization potential, the mass should not be affected by the latter error.

In summary, we find that all mass values in this experiment should be increased by about $0.7\ m_e$ to correct for small errors in the range-momentum relations[11] that were used. This correction appears in Table III.

---

[27] W. H. Barkas (private communication).

3. Deviation of the average mass from the true mass. Equation (22) indicates the behavior of the mass values determined as a function of the meson range R and momentum p. Symmetric distributions in R (straggling) and p_K (finite target thickness) thus lead to a small asymmetry in the mass distribution, and hence, to a deviation of the average value of the mass from the true mass. A calculation based on Eq. (22) and good to the second order in small variations of R and p yielded $\langle M \rangle - M_0 = +0.2\ m_e$, where $\langle M \rangle$ is the average obtained by our method and M_0 the true mass.

The average mass given by the predicted mass distribution (Fig. 9) was computed to be $0.3\ m_e$ higher than M_0, in good agreement with the above calculated results. Choosing the value obtained from the predicted distribution as the more reliable, we then must lower all average mass values by $0.3\ m_e$, as indicated in Table III.

4. Correction for emulsion density. The measured density of the emulsion was 3.80 ± 0.02 g/cm^3. Barkas and Young's tables[13] were based on an emulsion density of 3.815 g/cm^3. In order to be valid for the measured density, all ranges in the tables should be increased by $0.04\pm0.05\%$. From Eq. (26) and $M = 965\ m_e$ it follows that all masses should be increased by $0.04\pm0.5\ m_e$, as has been done in Table III.

5. Acceptance of inelastically scattered particles. An examination of the entrance angles and positions of all τ's and $K_\mu 2$'s indicated that a significant fraction of the abnormally high mass values may have resulted from particles having scattered off the pole pieces; others may have experienced inelastic collisions in the emulsion. If this was true, none of these events should have been included in the mass averaging, and the mass cutoff was justified. There may have been cases similar to these, whose mass values still lay within the acceptance limits, thus affecting the average mass in spite of the cutoff procedure. In an attempt to determine the result of their inclusion, it was assumed that the distribution of these events was of constant density from the average mass value to the point at $1100\ m_e$. The density was taken from the points lying outside the curve in Fig. 9. Such a distribution would have increased the average value by $0.5\ m_e$. A correction of $-0.5\pm0.5\ m_e$ has been included in Table III to account for this effect.